ELSEVIER

Tribology International 39 (2006) 62–69

TRIBOLOGY INTERNATIONAL

www.elsevier.com/locate/triboint

Nanoscratch and friction: An innovative approach to understand the tribological behaviour of poly(amide) fibres

J. Cayer-Barrioz[a,*], D. Mazuyer[a], A. Tonck[a], Ph. Kapsa[a], A. Chateauminois[b]

[a]*Laboratoire de Tribologie et de Dynamique des Systèmes, UMR 5513, Ecole Centrale de Lyon, 36 avenue Guy de Collongue—69130 Ecully, France*
[b]*Laboratoire de Physique Chimie des Polymères et des Milieux Dispersés, UMR 7615, ESPCI, 10 rue Vauquelin—75231 Paris, France*

Available online 6 June 2005

Abstract

The analysis of the wear resistance of polymeric fibres requires a better understanding of both their abrasive scratch behaviour and their frictional response. These aspects have been investigated at the nanometre scale using the resources of a modified surface force apparatus. In an attempt to simulate the abrasive wear losses, nanomachining experiments have been carried out which consists in the repeated scratching of a portion of the fibre surface by the rigid indenter. However, an analysis of the resulting surface topography indicated a significant plastic grooving of the fibre surface with no evidence of wear losses as it was observed at the macroscopic scale. Single pass nanoscratch experiments realised at various sliding speeds also allow discussing the relative contributions of both the material viscoplasticity and the tip/material local interactions on the frictional response. When the sliding speed was incrementally changed during a scratch experiment, it was observed that the associated friction variation was accommodated on a 50 nm distance, independently of the sliding speed.

Keywords: Friction; Nanoscratch; Nanotribology; Poly(amide) fibre

1. Introduction

Over the past years, the tribological behaviour of polymeric materials has drawn a considerable interest. Polymers' tribological performance is particularly relevant in the field of textile applications, where friction and wear properties are important aspects during both fibre processing and end-using. Even if poly(amide) fibres have emerged as an interesting alternative to natural fibres (such as cotton and wool), their surfaces remain highly sensitive to scratches. Such damage shortens the fibre life, and therefore, hinders their use for high performance textile structures.

A detailed investigation [1,2] of the wear mechanisms of poly(amide) fibres was previously carried out using a tribometer simulating the fibre abrasion processes at the macroscopic scale. The damaged contact zone on the fibre presents numerous abrasive scratches which are aligned along the sliding direction, as shown in Fig. 1. At the macroscopic scale, very important volumetric wear losses are measured. The detailed analysis of such abrasive processes is, however, much complicated by the multiple dynamic asperity interactions involved in macroscopic contacts between the rough surfaces. In order to bypass these difficulties, indentation and scratching experiments have long been recognized as a potential route to mimic and characterize in a more controlled manner the deformation and failure modes involved in asperity engagements [3].

Most existing models describing the scratch properties of materials consider a moving hard tip grooving the surface, but they do not take into account the viscoelastic and/or viscoplastic effects which can be significant in the case of polymeric materials [4–6]. The early description of Bowden and Tabor [4] assumed that the tangential load necessary to move a grooving tip laterally under a constant normal load is the sum of two separate components, namely an interfacial shear component (often denoted to as the 'adhesive' component of friction) and a bulk ploughing term. As a first approximation, these two components were assumed to be non-interactive. Recent experiments using the resources of in situ visualization demonstrated, however, that strong interactions between the interface and ploughing components can be involved during the scratching of viscoelastic polymers [7]. Such effects are especially

* Corresponding author. Tel.: +33 4721 86288; fax: +33 4784 33383.
E-mail address: juliette.cayer-barrioz@ec-lyon.fr (J. Cayer-Barrioz).

0301-679X/$ - see front matter © 2005 Elsevier Ltd. All rights reserved.
doi:10.1016/j.triboint.2005.04.010

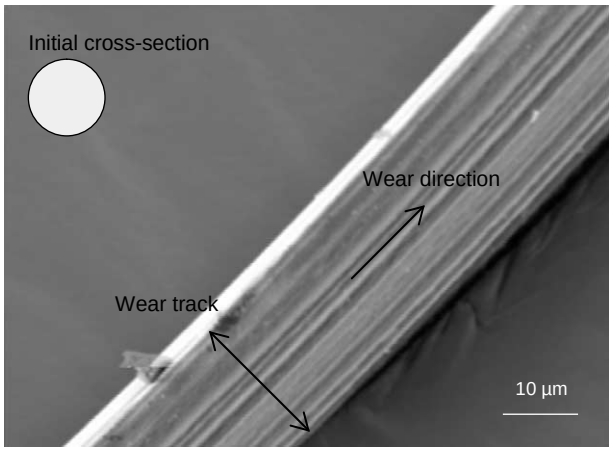

Fig. 1. SEM observations of worn polyamide fibres ($M_n = 19$ kg/mol) under abrasive conditions (for a sliding distance of 50 m). Abrasive scratches are aligned parallel to the sliding direction. Extensive plastic deformation at the fibre surface is noticed. The shape of the initial cross-section of the fibre is also depicted.

demonstrated through the investigation of the dependence of the shape and size of the contact area on parameters such as sliding speed or temperature.

The analysis of scratch behaviour is critically dependent upon the estimate of the size and shape of the contact area. The true contact area between the moving tip and the material is somewhat difficult to predict, and is therefore, generally considered to be the front half of the part of the tip in contact with the surface [7]. In the case of viscoelastoplastic materials, some contact between the tip and the polymeric surface can occur in the trailing zone of the contact by virtue of the elastic recovery of the material. In such a situation, the ploughing term of the friction force only depends on the attack angle (the asperity slope angle) of the tip and on this partial elastic recovery [8]. It remains nevertheless extremely difficult to accurately estimate the interfacial friction component in situations such as scratching, where extensive bulk ploughing mechanisms are involved.

Most existing models were developed for the scratching of perfectly plastic materials using conical tips [9,10]. These models are usually developed assuming an Amontons–Coulomb's friction law at the interface [11] and stationary sliding conditions. In the context of polymeric materials, two attempts to estimate the interfacial friction component are noteworthy: Bucaille et al. [12] adapted the Tabor's model, whereas Lafaye [10] proposed a method based on a three dimensional flow line description. However, the latter require an accurate knowledge of the elastic recovery of the material.

The goal of this paper is to investigate the deformation modes and the friction processes involved during the scratching of oriented polymeric fibres at the nanoscale, in order to get a better insight into the wear mechanisms observed at the macroscopic scale. An innovative approach was used, where the study of scratch formation was combined with an analysis of the frictional response of the polymeric fibres. A method associating imaging procedures with nanoscratch experiments was developed on the basis of a modified Surface Force Apparatus [13]. This technique was first used to investigate the nanomachining of the fibre surface and to quantify the associated wear at the nanoscale. In a second step, an analysis of the frictional response of the fibre was carried out by means of nanoscratch tests performed at various sliding speeds. This leads to discuss the role of the interfacial friction and to propose an interpretation of the contact behaviour in terms of interfacial rheology.

2. Experimental details

2.1. Materials

The polymeric fibres investigated in this study were supplied by Rhodia (Saint-Fons, France). Specimens, made of thermoplastic semi-crystalline poly(amide) 6, were elaborated by melt spinning followed by an additional hot drawing step [14] in order to achieve the required draw ratio of three. This manufacturing process is associated with the development of a microfibrillar structure which can be described using the morphological 'swiss-cheese' model proposed by Prevorsek [15,16]. In this model, the fibres are composed of periodic series of crystallites and amorphous domains, called microfibrils, which are embedded in an oriented amorphous matrix, as illustrated in Fig. 2. The molecular weight, M_n, of the specimens measured using size exclusion chromatography in dichloromethane is about 19 kg/mol. The fibre round section has a mean diameter of 42 µm. The mechanical properties of the fibres (Young's modulus in the radial and the tangential directions and the hardness) were determined by nano-indentation

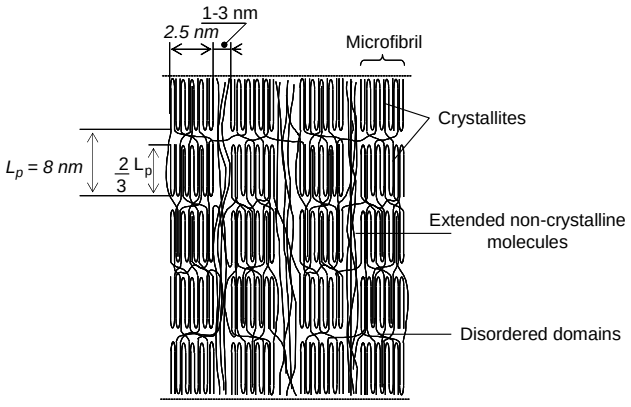

Fig. 2. The Prevorsek's 'Swiss-cheese' structural model of poly(amide) 6 fibres (from Refs. [15,16]). The fibre axis is vertical. Crystallites are periodically organised to form microfibrils, which are embedded in an amorphous oriented matrix. Molecular parameters such as the diameter of the microfibrils, their periodic lengths and the width of the amorphous disordered domains are taken from the literature [16] and SAXS measurements.

experiments [17] at 300 K and a zero relative humidity: the reduced Young's modulus in the radial (respectively, tangential) direction is about 1.8×10^9 Pa (respectively, 2.7×10^9 Pa) while the hardness reaches 10^8 Pa. The fibre glass transition temperature, estimated by differential scanning calorimetry at 1.6 K/s is around 333 K at a zero relative humidity.

2.2. Nanoscratching using a surface force apparatus

The nanoscratch experiments were carried out using the Ecole Centrale de Lyon Surface Force Apparatus (SFA) which was already described in the literature [13,17]. The principle of the SFA is shown schematically in Fig. 3.

A diamond tip can be moved towards and away from a plane sample holder. The use of the expansion and the vibration of three piezoelectric actuators, controlled by three specifically designed capacitive sensors, allows accurate displacement control along the three axes x, y (parallel to the plane sample holder) and z (normal to the plane sample holder): the sensitivity of the displacements is 10^{-2} nm in each direction. High resolution and compliant (up to 2×10^{-6} m/N) capacitive sensors equip double cantilever sensors, which are supporting the sample holder. The latter allow measuring the quasi-static normal and tangential forces (respectively, F_z and F_x) with a resolution up to 10^{-8} N. Three closed feedback loops are used to control the high voltage amplifiers associated with the piezoelectric actuators. Two displacement closed feedback loops allow controlling the tangential displacements x and y while the operations in the normal direction z can be carried out either in displacement or normal force control [18]. The scratch experiment can then be made either at constant penetration depth or at constant normal load. Using the z feedback control in the constant force mode, the surface topography can be imaged with the diamond tip before and after scratching.

2.3. Experimental methodology

Nanoscratch experiments were performed at room temperature. A trigonal diamond tips with an angle of 90° between edges was used. The tip defect, determined according to a precise calibration procedure detailed in [19,20], was estimated to be about 16 nm. The studied fibres were maintained along their longitudinal axis on a flat sample holder by means of a carbon pellet. Prior to the experiments, the tip must be accurately located at the top of the curved fibre surface. In such a situation, the normal displacement axis, z, corresponds to the radial direction of the fibre and the tangential direction, x, is parallel to the fibre longitudinal axis. Two kinds of experiments were performed:

(a) First, the elementary wear processes of the fibre were investigated by the nanomachining of the surface: an area scratching, consisting in 256 parallel scratches of 1 μm long with a spacing of 4 nm between each other was performed; this area scratching procedure was repeated for four times over the same portion of the fibre. The principle of the experiment is illustrated in Fig. 4. The scratching speed was 400 nm/s and the scratching was made in the constant penetration mode with a penetration depth of 100 nm with the tip faced forward [13]. The in situ imaging of the nanomachined surface allows quantifying the wear volume generated by the repeated sliding of the tip. During the nanomachining procedure, both the tangential and the normal forces were continuously recorded. The combined

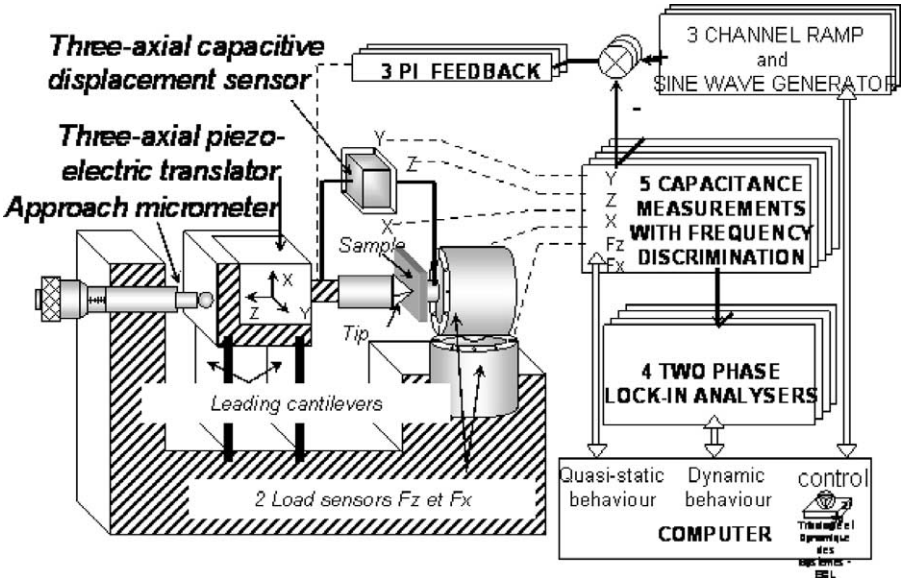

Fig. 3. Schematic diagram of the surface force apparatus.

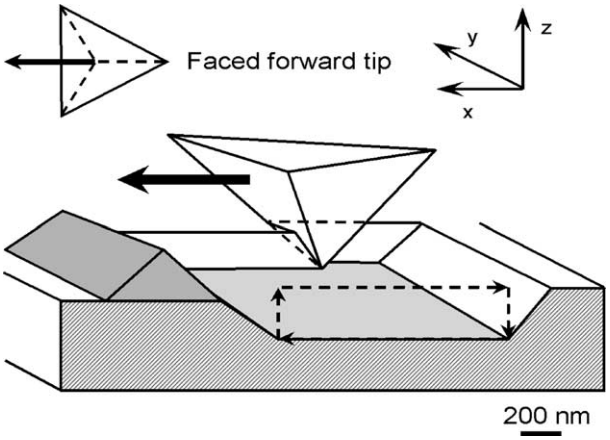

Fig. 4. Schematic description of the nanomachining procedure used to investigate the nanoscale wear processes of the fibres.

measurements of forces and worn volume allow the calculation of the dissipated energy.

(b) Single scratch experiments (parallel to the tangential direction, x) of the edged forward tip on the fibre surface at a controlled normal force of 24 μN and at low speed (between 0.7 and 14 nm/s) were carried out in order to study the friction between the tip and the polymeric fibre. During the tests, the normal, F_z, and tangential, F_x, forces were recorded, which allowed to calculate the apparent friction coefficient, μ_{app}, defined as:

$$\mu_{app} = \frac{F_x}{F_z} \quad (1)$$

The mechanical behaviour of poly(amide) materials is known to be highly sensitive to water plasticization effects [21–24]. During water diffusion, the plasticization of the poly(amide) amorphous phase induces a significant decrease in elastic and plastic properties, by virtue of a shift of the glass transition below room temperature [22]. In order to reduce the effects of variable moisture on poly(amide), the fibres were first dried for 12 h under vacuum at 10^{-9} bar and then exposed to nitrogen at 1 bar during the experiments.

3. Results and discussion

The first part of this section presents the analysis of nanowear processes as determined from the nanomachining experiments. The results regarding the frictional behaviour of the polymeric fibres and the influence of the scratching velocity are discussed in the following parts.

3.1. Nanowear analysis

In order to estimate the microscopic wear rate associated with the repeated sliding of an asperity, four successive nanomachining scans were performed at the surface of the polymeric fibres. Fig. 5 presents an image of the resulting fibre surface. A large frontal pile-up can be observed as well as some more limited lateral pile-up. The wear volume, V_{wear}, defined as the difference between the grooved volume, V_-, and the pile-up volume, V_+, can be estimated [25] from topographic measurements along the sliding direction, x, as shown Fig. 6, and along the direction y. V_+ and V_- are defined from a reference plane which corresponds to the initial surface of the fibre before the machining test. Both front, rear and lateral pile-up were taken into account in the calculation of V_+. The resulting wear volume, V_{wear}, after four successive nanomachining experiments of the surface is close to zero. The polymeric material is clearly plastically deformed and displaced around the tip, but is not abraded by the scratching process.

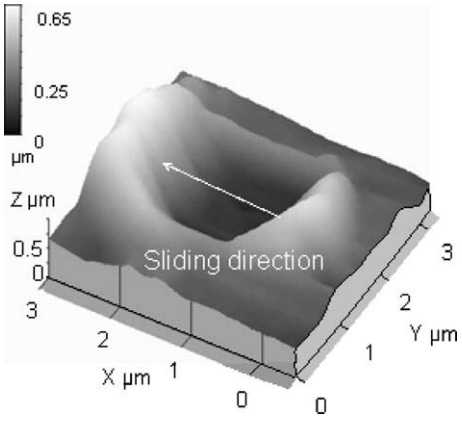

Fig. 5. Three-dimensional topographic image of the fibre surface after four successive nanomachining paths. The sliding direction is along the x direction. Large frontal and minor lateral pile-up are observed.

During a nanomachining experiment, the order of magnitude of the dissipated energy, E_T, and the order of magnitude of the energy used for the plastic deformation, E_p, can be calculated from

$$E_T = F_x \times L \times N \approx 3 \times 10^{-8}\ \text{J} \quad (2)$$

$$E_p = H \times V_- \approx 2 \times 10^{-10}\ \text{J} \quad (3)$$

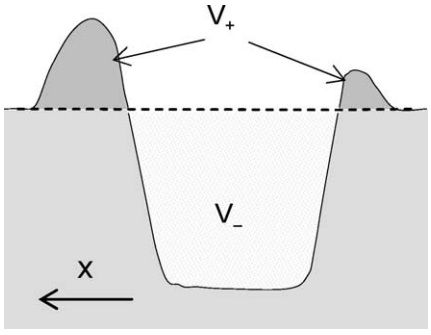

Fig. 6. Calculation of the wear volume, V_{wear}, from the knowledge of the surface profile. V_+ (respectively, V_-) represents the volume of material in the frontal pile-up (respectively, the grooved volume).

where F_x is the average tangential force (an appropriate order of magnitude is 30 μN), L is the length of the scratch (i.e. 1 μm), N is the number of scratches (i.e. 1024) and H is the hardness of the polymer. Since $E_p \ll E_T$, it can be deduced that the major part of the energy is probably dissipated in the interfacial friction process. At the macroscopic scale, a wear process is noticed, associated with major material losses [1,2]. Therefore, it may be supposed that at the nanoscale, the dissipated mechanical energy is too low to result in material removal, although all the energy is not only used for the plastic deformation, but also in the interfacial friction process. Moreover, even if the trigonal indenter is well representative of the geometry of the abrasive asperities, the strain rates are much lower than the ones used in the macroscopic wear process (due to the strong difference between the sliding speeds at both scales).

Before and after each nanomachining experiment, nano-indentation tests at 10 μN were performed on the polymer surface at a penetration rate of 1 nm/s. The nano-indentation procedure is described in detail in [17]. From these tests, it was concluded that the mechanical properties of the polymer surface in terms of modulus and hardness are not significantly modified by the nanomachining process. However, nano-indentation tests reveal a modification of the fibre surface: although no adhesive pull-off force was detected on the original surface, a low adhesive pull-off force (about 0.05 μN) appears during the unloading stage following the first nanomachining experiment. This indicates that dissipative and/or adhesive properties of the polymeric surfaces are modified due to the sliding of the asperities.

3.2. Nanofriction experiments at constant sliding speed

A preliminary nano-indentation step was realised at 30 μN and for a loading speed of 1 nm/s in the controlled displacement mode. After the relaxation of the indentation force, nanoscratch experiments were conducted at 14 nm/s, with the edged forward tip in the tangential direction, x, at a controlled normal force of 24 μN. Fig. 7 shows the evolution of the tangential force, F_x, and of the tip penetration depth, h, versus the sliding distance normalized with respect to the contact half length, a. By virtue of geometric considerations, the latter is estimated as follows for a trigonal tip:

$$a = 0.90 \times h \tag{4}$$

In order to compare the observed behaviour to other typical scratching responses, a schematic evolution of the tangential force and of the tip penetration depth, for a purely plastic and a viscoplastic isotropic materials is also presented in Fig. 7. The behaviour of the viscoelastoplastic fibres strongly differs from that of plastic and viscoplastic isotropic materials: in the case of the viscoelastoplastic fibres, the tangential force reaches a maximum and then decreases while it should remain constant within the frame of a plastic

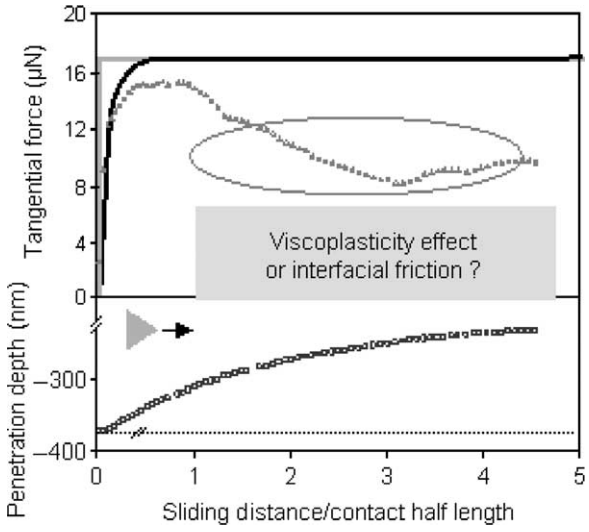

Fig. 7. Evolution of both the tangential force, F_x, and the penetration depth, h, versus the ratio of the sliding distance to the contact half length during a nanoscratch realised with the edged forward tip and for a normal controlled force F_z of 24 μN. (Δ) F_x, (□) h for the viscoelastoplastic PA6 fibres. Theoretical curves of the tangential force and of the penetration depth are also given for perfectly plastic and viscoplastic materials. (grey —) F_x for perfectly plastic material, (black —) F_x for viscoplastic material, (■■) penetration depth for perfectly plastic and viscoplastic materials.

or viscoplastic behaviour. Moreover, the tip penetration depth also varies with the sliding distance: the tip is pushed out of the surface, which is unexpected since the creep of the contact would rather make the penetration depth increase. Neither the penetration depth nor friction reaches a stationary value within the considered sliding distance. During nanoscratch experiments, the tangential force results from an interface frictional component characterizing the relative sliding of two surfaces without any bulk material deformation and from a ploughing component attributed to the viscoelastic and/or viscoplastic flow of the material around the tip. As a consequence, the variations of the tangential force and of the penetration depth can be due either to the viscoelastoplasticity of the bulk poly(amide) or to the variation of the interfacial frictional response.

One can also wonder the effects of the interactions between bulk viscoplasticity and interface friction on the fluctuations of the penetration depth. During the incipient stages of sliding, the polymeric material in the contact zone undergoes contradictory effects:

- An increase in the mean deformation rate which is likely to be associated with enhanced elastoplastic properties. This in turn will induce a decrease in the contact area, and hence, a decrease in the penetration depth.
- During scratching, polymeric material flow is forced downwards and outwards into the surrounding hinterland which expands. It can be assumed that the energy dissipated to push the material is higher than the one required to climb over the polymeric ‘wave’. This also results in a diminution of the penetration depth.

– In contrast, the creep of the contact leads to an augmentation of the penetration depth.

These effects are interactive and they result in variations of the penetration depth, as illustrated in Fig. 7.

3.3. Identification of the preponderant contribution

In this paper, an attempt is made to identify the relative contributions of interface shear and bulk ploughing to the friction force by conducting scratch tests at variable sliding speeds. Nanoscratch tests were carried out in a range of sliding speeds varying between 0.7 and 14 nm/s with the edged forward tip. The sliding speed initially equal to 0.7 nm/s was increased to 3.5 nm/s and then to 14 nm/s before decreasing following the opposite procedure. The friction experiments were conducted by keeping the normal force, F_z, constant at 24 μN. The variations of the tangential force, F_x, and of the tip penetration depth, h, with time are shown in Fig. 8. Due to the very low tangential compliance of the apparatus and the large displacement resolution, the tangential compliance of the material itself and the variations of the tangential force, F_x, are detected [26]. Fig. 8 gives rise to three main observations:

– the tangential force fluctuations are accommodated by penetration depth variations,
– the tangential force depends on the sliding speed, which is in striking contrast with the Amontons–Coulomb laws of friction,
– the shape of the transient peaks generated at each speed change differs as a function of the considered sliding distance, in particular below and beyond a sliding distance corresponding to one contact half length (approximately 300 nm). The following paragraphs present in more details these transient peaks and their interpretation as a function of the sliding distance.

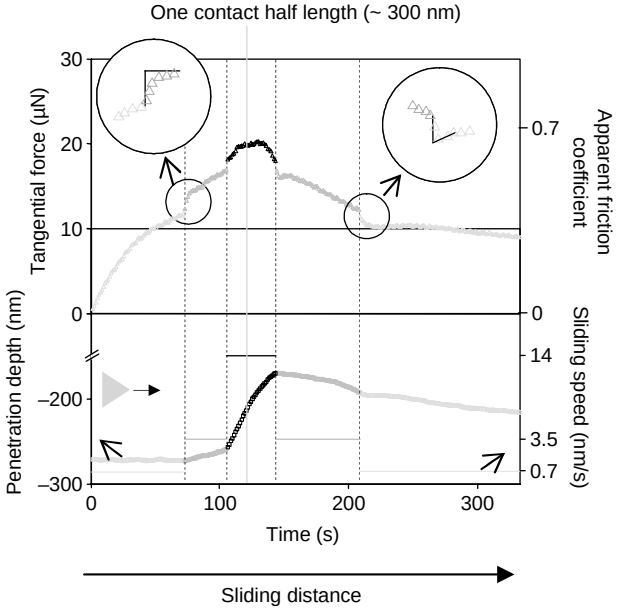

Fig. 8. Influence of the sliding speed on the tangential force and the penetration depth during a nanoscratch at an imposed normal force $F_z = 24$ μN, with the edged forward tip. The sliding speed varies from 0.7 to 14 nm/s. (Δ) Tangential force F_x, (□) penetration depth h, (—) sliding speed.

3.3.1. Sliding distance inferior to one contact half length

During this first stage, the evolutions of the tangential forces as a result of a velocity change are related to the polymer viscoplasticity (Fig. 8): the speed increase is associated with a significant augmentation of the tangential force (which is typical of a viscoplastic effect) and then with a slower variation related to the pile-up formation around the tip. The apparent friction coefficient reaches 0.64 (Fig. 8), which approximately corresponds to the ploughing of the surface (tan $\beta = 0.7$, where β is the attack angle presented by the edged forward indenter). The small difference between theoretical and experimental values can be attributed to a slight rotation of the tip axis relative to the direction of the fibre axis. This clearly demonstrates the preponderance, during this first stage, of the bulk viscoplasticity—a time accommodated process—on the tip/material local interactions.

3.3.2. Sliding distance greater than one contact half length

Beyond one contact half length, the evolutions of the forces as a result of a change in the sliding speed can no longer be attributed to the bulk viscoplasticity: the associated transient peak in the tangential load exhibits a first direct effect, consisting of a decrease in the tangential force with decreasing speed, followed by a relaxation step to reach a stabilized value (Fig. 8).

In an attempt to differentiate between the contribution of bulk ploughing and interface shear to the velocity dependence of the frictional force, two successive scratches, with the edged forward indenter, were realised inside a previously formed scar. This entails a better characterization of the interfacial friction between the tip and the surface since the formation of the viscoplastic groove and the associated pile-up is mainly achieved during the first scratch. At first, the sliding speed was maintained at 14 nm/s. Beyond a sliding distance corresponding to one contact half length, the speed was decreased to 3.5 nm/s, then 0.7 nm/s before being increased following the opposite procedure. Fig. 9 shows the evolution of the tangential force and of the penetration depth versus the sliding distance, for a controlled normal force of 24 μN during the third scratch. Beyond one contact half length, the shape of the transient peak associated with a speed modification (Fig. 9) remains similar to that observed during the first scratch. Moreover, it is noteworthy that the relationship between the speed and the tangential force is reversible since it is observed during both a sequential speed increase or decrease procedure. Such a non-Coulombic behaviour can thus be interpreted

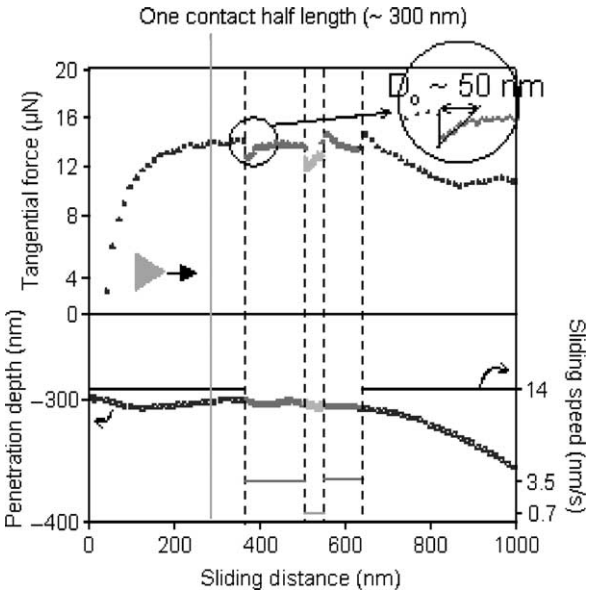

Fig. 9. Changes in the tangential force (Δ) and of the penetration depth (□) as a function of the sliding distance, during the third nanoscratch carried out inside the same groove on the fibre surface (edged forward tip, normal force of 24 μN). The sliding speed ranges from 0.7 to 14 nm/s. Beyond a sliding distance of one contact half length (approximately 300 nm), the tip/material local frictional interactions are preponderant on bulk viscoplastic ploughing. At each velocity change, an accommodation of the frictional processes is observed over a distance of about 50 nm independently of the sliding speed (insert).

in terms of an interfacial accommodation of the sliding speed [27]. An accommodation distance, D_0, independent of the sliding speed and close to 50 nm, can be ascribed to this process. Similar accommodation stages were also observed during scratch tests carried out with the faced forward tip. As a consequence, they are independent of the tip attack angle, and therefore, of the ploughing contribution.

According to Baumberger et al. [27–29], this accommodation distance, D_0, can be attributed to the average memory length necessary to slip to refresh the microcontact population in a sliding multi-asperity contact. The accommodation time is then attributed to the microcontact ageing. However, similar effects have also been observed for single asperity contacts [26,30] which indicates that they must be essentially considered as a signature of the interface rheology, independently of considerations associated with surface topography.

3.4. Analysis of the interface rheology

Nanoscratch experiments show that the friction coefficient does not follow the Amontons–Coulomb's laws of friction and depends in particular on the sliding velocity, V. It is known from many studies [27–29,31] that, in the low sliding velocity regime (typically $V < 100$ μm/s), the steady sliding of a multicontact interface is characterized by a 'velocity weakening' behaviour. For most studied materials,

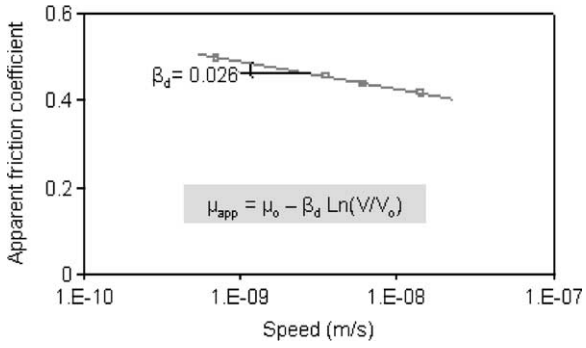

Fig. 10. Linear evolution of the apparent friction coefficient, μ_{app}, with the sliding speed in logarithmic scale, typical of a velocity weakening regime. The slope of the linear relationship, β_d, is about 0.026 which is in good agreement with the literature [27].

one measures, to a good approximation:

$$\mu_{app} = \mu_0 - \beta_d \times \ln(V/V_0) \quad (5)$$

where μ_0 is the friction coefficient corresponding to a sliding velocity V_0, and β_d is the slope. The friction coefficient was measured beyond a sliding distance of one contact half length at two different sliding speeds during the second or third consecutive scratch:

- μ_{app} ($V = 14$ nm/s) = 0.42,
- μ_{app} ($V = 0.7$ nm/s) = 0.5.

Therefore, the relation (5) is experimentally fitted for a slope $\beta_d \sim 0.26$ at room temperature, which is in good agreement with the value found in the literature [27]. From this relation, the apparent friction coefficient can be calculated as a function of the sliding velocity (Fig. 10). In this low sliding velocity regime, the relation μ_{app} (V) with a negative slope induces an amplification of every fluctuation of speed around its stationary value: a deceleration leads to an increase in the friction force, hence to further deceleration.

Despite the monocontact nature of the interface, it may be assumed that this relation can also be applied to the case investigated in this paper: friction phenomena are found to be accommodated on a distance, D_0, independent of the sliding speed and the existence of this accommodation distance is mentioned in the literature for mono or multicontact interface and various materials.

4. Conclusions

An investigation of the wear of poly(amide) 6 fibres at the nanometre scale was performed by the nanoscratch experiments between a single fibre and a trigonal indenter using a Surface Force Apparatus. The nanomachining of the polymeric surface resulted in the plastic flow of the material and did not imply any material loss at this scale.

This difference with the abrasive processes observed at the macroscopic scale was tentatively attributed to the much lower strain rates achieved during nanoscratching. Although the nanomachining process did not induce significant changes in the polymer mechanical properties, it modified the surface dissipative and/or adhesive properties. Energetic calculations showed that a major part of the frictional energy was dissipated by interface frictional process.

Nanoscratch experiments clearly demonstrated that the apparent friction coefficient did not follow the Coulomb's laws since they gave strong evidence of a correlation between the indenter penetration, the sliding speed and the tangential force. In spite of complex interactions between bulk viscoplasticity and interfacial friction, it was possible to determine the relative contributions of these processes to the measured friction coefficient, even if the stationary friction regime was not completely achieved. Whereas the viscoplasticity, a time accommodated process, was preponderant during pile-up formation, the interfacial friction became prevalent beyond one contact half length, after formation of the pile-up. During this stage, change in the sliding velocity were accommodated within a characteristic length of about 50 nm, independently of the sliding speed. This accommodation length was attributed to the rheology of the interface zone.

Acknowledgements

The authors are indebted to F. Bouquerel from Rhodia Technical Fibres for financial assistance and for providing the studied materials. We also thank G. Robert from Rhodia Recherches.

References

[1] Cayer-Barrioz J, Mazuyer D, Kapsa Ph, Chateauminois A, Bouquerel F. On the mechanisms of abrasive wear of polyamide fibres. Wear 2003;255:751–7.
[2] Cayer-Barrioz J, Mazuyer D, Kapsa Ph, Chateauminois A, Robert G. Abrasive wear micromechanisms of oriented polymers. Polymer 2004;45:2729–36.
[3] Briscoe BJ. Isolated contact stress deformations of polymers: the basis for interpreting polymer tribology. Tribol Int 1998;31(1–3):121–6.
[4] Bowden FP, Tabor D. Friction and lubrication of solids. London: Oxford University Press; 1951.
[5] Rabinowicz E. Friction and wear of materials. New York: Wiley; 1965.
[6] Williams JA. Analytical models of scratch hardness. Tribol Int 1996; 29(8):675–94.
[7] Gauthier C, Lafaye S, Schirrer R. Elastic recovery of a scratch in a polymeric surface: experiments and analysis. Tribol Int 2001;34: 469–74.
[8] Cayer-Barrioz J. Mécanismes d'usure de polymères orientés: application à l'abrasion des fibres de polyamide. PhD thesis, Ecole Centrale de Lyon; 2003. p. 2003–32.
[9] Bucaille JL, Felder E. L'essai de rayure sur polymères et métaux: modélisations et approaches expérimentales. Matériaux et techniques 2001;3-4:29–43.
[10] Lafaye S. Propriétés mécaniques de friction et de déformation des surfaces de polymères solids. PhD thesis, Université de Strasbourg; 2002.
[11] Georges JM. Frottement, usure et lubrification. Paris: CNRS Editions; 2000.
[12] Bucaille JL, Felder E, Hochstetter G. Mechanical analysis of the scratch test on elastic and perfectly plastic materials with the 3-dimensional finite element modeling. Wear 2001;249:422–32.
[13] Tonck A, Bec S, Mazuyer D, Georges JM, Lubrecht AA. The Ecole Centrale de Lyon surface force apparatus: an application overview. Proc Inst Mech Eng 1999;213:353–61.
[14] Penning JP, Van Ruiten J, Brouwer R, Gabriëlse W. Orientation and structure development in melt-spun nylon 6 fibres. Polymer 2003;44: 5869–76.
[15] Bukosek V, Prevorsek DC. Model of nylon 6 fibres microstructure: microfibrillar model or 'swiss-cheese' model? Int J Polym Mater 2000;47:569–92.
[16] Prevorsek DC, Harget PJ, Sharma RK, Reimschuessel AC. Nylon 6 fibers: changes in structure between moderate and high draw ratios. J Macromol Sci Phys 1973;B8:127–56.
[17] Cayer-Barrioz J, Tonck A, Mazuyer D, Kapsa Ph, Chateauminois A. Nanoscale mechanical characterization of polymeric fibres. J Polym Sci: Part B: Polym Phys 2005.
[18] Bec S, Tonck A, Georges JM, Georges E, Loubet JL. Improvements in the indentation method with a surface force apparatus. Philos Mag A 1996;74(5):1061–72.
[19] Briscoe BJ, Sebastian KS, Adams MJ. The effect of indenter geometry on the elastic response to indentation. J Phys D: Appl Phys 1994;27: 1156–62.
[20] Odoni L. Propriétés mécaniques et effects d'échelle. PhD thesis, Ecole Centrale de Lyon 1999;99–17.
[21] Hernandez RJ, Gavara R. Sorption and transport of water in nylon 6 films. J Polym Sci: Part B: Polym Phys 1994;32:2367–74.
[22] Kohan MI, editor. Nylon plastics handbook. Munchen: Hanser; 1995.
[23] Stuart B, Briscoe BJ. Surface plasticisation of nylon 66 by water. Polym Int 1995;38:95–9.
[24] Valentin D, Paray F. Guetta B.The hygrothermal behaviour of glass fibre reinforced PA66 composites: a study of the effect of water desorption on their mechanical properties. J Mater Sci 1987;22:46–56.
[25] Kato K. Wear mechanisms. Proceedings of the first World Tribology Congress.: Mechanical Engineering Publications; 1997. p. 39–56.
[26] Georges JM, Tonck A, Mazuyer D. Interfacial friction of wetted monolayers. Wear 1994;175:59–62.
[27] Bureau L. Elasticité et rhéologie d'une interface macroscopique: du piégeage au frottement solide. PhD thesis, Université Paris VII; 2002.
[28] Baumberger T. Contact dynamics and friction at a solid-solid interface: material versus statistical aspects. Solid State Commun 1997;102(2-3):175–85.
[29] Bureau L, Baumberger T, Caroli C. Rheological ageing and rejuvenation in solid friction contacts. Eur Phys JE 2002;8:331–7.
[30] Mazuyer D, Tonck A, Bec S, Loubet JL. Nanoscale surface rheology in tribology. In: Tribology series, tribology research: from model experiment to industrial problems, vol. 39. Amsterdam: Elsevier; 2001. p. 273–82.
[31] Bureau L, Baumberger T, Caroli C, Ronsin O. Low velocity friction between macroscopic solids. CR Acad Sci Paris 2001;2(IV):699–707.